Tuning the transport behavior of centimeter-scale WTe_2 ultrathin films fabricated by pulsed laser deposition

Ming Gao, Minhao Zhang, Wei Niu, Yequan Chen, Min Gu, Haoyu Wang, Fengqi Song, Peng Wang, Shicheng Yan, Fengqiu Wang, Xinran Wang, Xuefeng Wang, Yongbing Xu, and Rong Zhang

Citation: Appl. Phys. Lett. **111**, 031906 (2017); doi: 10.1063/1.4995227
View online: http://dx.doi.org/10.1063/1.4995227
View Table of Contents: http://aip.scitation.org/toc/apl/111/3
Published by the American Institute of Physics

Tuning the transport behavior of centimeter-scale WTe_2 ultrathin films fabricated by pulsed laser deposition

Ming Gao,[1,a)] Minhao Zhang,[1,a)] Wei Niu,[1] Yequan Chen,[1] Min Gu,[2] Haoyu Wang,[2,3] Fengqi Song,[3] Peng Wang,[2] Shicheng Yan,[2] Fengqiu Wang,[1] Xinran Wang,[1] Xuefeng Wang,[1,b)] Yongbing Xu,[1] and Rong Zhang[1]

[1]*National Laboratory of Solid State Microstructures, Collaborative Innovation Center of Advanced Microstructures, School of Electronic Science and Engineering, Nanjing University, Nanjing 210093, People's Republic of China*

[2]*College of Engineering and Applied Sciences, Nanjing University, Nanjing 210093, People's Republic of China*

[3]*School of Physics, Nanjing University, Nanjing 210093, People's Republic of China*

(Received 15 May 2017; accepted 6 July 2017; published online 20 July 2017)

We report on an avenue to obtain the centimeter-scale, uniform, and high-quality WTe_2 ultrathin films by a pulsed laser deposition technique and the post-annealing under the tellurium (Te) vapor. The WTe_2 ultrathin films showed the typical metallic behavior when Te vacancies were mostly eliminated. Magnetoresistance measurements showed that WTe_2 ultrathin films underwent the competition between weak localization and weak antilocalization that could be modulated by the amount of Te vacancies. Our study may open an avenue to improve the charge transport of WTe_2 for its two-dimensional device applications. *Published by AIP Publishing.*
[http://dx.doi.org/10.1063/1.4995227]

WTe_2, one of two-dimensional (2D) layered materials, is a unique transition-metal dichalcogenide (TMD) semimetal with a distorted 1T structure (Td).[1] Bulk WTe_2 was revealed to host the large unsaturated magnetoresistance (MR) property,[1] which is commonly believed to stem from the full compensation of electron and hole pockets[1–4] and the spin-orbit coupling.[2] It has also been found to exhibit the exotic superconducting behavior under the high pressure.[5,6] More recently, it has been regarded as a Weyl semimetal candidate.[7]

Notably, few-layer TMDs often have different properties from bulk ones and exhibit extraordinary potential for both electronic and photonic applications.[8,9] WTe_2 exhibits the promising potential for spintronic, electronic, and optical applications. WTe_2 thin flakes can be used to generate femtosecond mode-locked laser pulses.[10] The control of spin-orbit torques by crystal symmetries was realized in WTe_2/ferromagnet bilayers.[11] WTe_2 thin films can also be used as the 2D metallic contacts for 2D semiconductors and was predicted to play a significant role in the field of tunneling field effect transistors.[12] Few-layer WTe_2 has been fabricated by mechanical exfoliation[13] and chemical vapor deposition (CVD)[14] and has been proved to remain the gapless semimetal.[13] However, WTe_2 exhibits the quite different transport behavior through reducing the thickness.[13] In addition, weak antilocalization was found in the few-layer WTe_2 sample,[13,14] and crossover from weak antilocalization to weak localization can be tuned by electrostatic gating.[14] To satisfy the requirement of the future potential device applications, exploring the fabrication method capable of providing the large-scale and high-yield ultrathin materials is of crucial importance.[15] As compared with the methods mentioned above, pulsed laser deposition (PLD) has its own advantages including the high growth rate, facile control of thickness and morphology, and relatively low growth temperature.[15] Till now, PLD has been used to fabricate several 2D materials such as graphene, black phosphorus, and TMDs.[15] Especially for TMDs, optical and electronic applications have been explored based on high-quality few layer MoS_2[16,17] and WS_2[18,19] fabricated by PLD.

In this letter, we fabricated the large-scale, uniform, and high-quality WTe_2 ultrathin films by the PLD method with a post-annealing procedure. Through controlling the annealing Te vapor pressure, we were able to improve the transport properties due to the elimination of the mostly Te vacancies. MR measurements showed that WTe_2 ultrathin films experienced the competition between weak localization and weak antilocalization, which can be modulated by the amount of Te vacancies.

The pre-reacted WTe_2 powder was used as the target material. It was prepared by heating the mixed tungsten (99.99%) and tellurium (99.99%) powders with a stoichiometric ratio of 1:2 at 700 °C for a week, which were sealed in the evacuated quartz tube using a turbomolecular pump. The thoroughly reacted WTe_2 powder was pressed into a hard target using a Dry Powder Press Machine and then further sintered at 700 °C in the sealed tube. The cleaned mica substrate ($1 \times 1\,cm^2$) was loaded into the PLD vacuum chamber (evacuated down to $\sim 4 \times 10^{-7}$ mbar) and positioned parallel to the WTe_2 target surface at a distance of ~5 cm. The films were deposited onto the substrate at 300 °C for 30 min using a 248 nm KrF excimer laser beam (an average fluency of 1.5 mJ/cm^2 and a repetition rate of 1 Hz). The as-prepared ultrathin films displayed the amorphous structure, and thus, the films were sealed in a 20 mL quartz tube with the added Te powder and annealed at 700 °C for 48 h to crystallize and improve the film structure. The amount of Te

[a)]M. Gao and M. Zhang contributed equally to this work.
[b)]Author to whom correspondence should be addressed: xfwang@nju.edu.cn

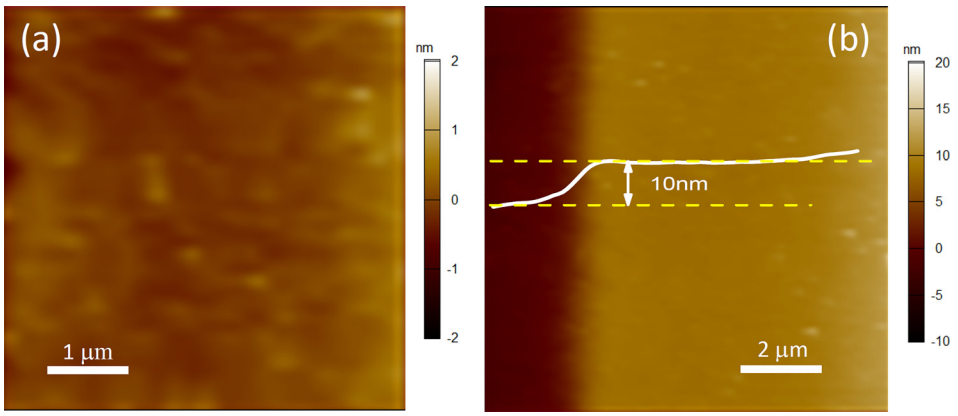

FIG. 1. Surface morphology and thickness of the WTe_2 ultrathin film. (a) AFM analysis of the surface roughness. (b) Thickness of the WTe_2 ultrathin film.

powder added was 0.0005 g, 0.0010 g, and 0.0025 g, and the corresponding ultrathin films were labelled as $WTe_{1.5}$, $WTe_{1.8}$, and WTe_2, respectively. Such a stoichiometry of these samples was determined by both X-ray photoemission spectroscopy (XPS) and energy dispersive spectroscopy (EDS) (see the supplementary material). The thickness and surface morphology were examined by the atomic force microscope (AFM) system (Asylum Cypher). The crystalline structure of these WTe_2 ultrathin films was determined by X-ray diffraction (XRD) using a Cu Kα line (Rigaku Ultima III) and a micro-Raman spectrometer (NT-MDT nanofinder-30) with a 514.5 nm Ar^+ laser. We also show more evidence that WTe_2 thin films possess the single-crystalline structures by transmission electron microscopy (TEM) (see the supplementary material). The transport properties were measured by a Quantum Design Physical Property Measurement System (PPMS-14 T).

Figure 1(a) shows the typical AFM image of the WTe_2 ultrathin film, indicating a high degree of uniformity over the large scale. The surface microstructure of the AFM image has a mean roughness of only 0.2 nm. The thickness of WTe_2 ultrathin film can be deduced from the AFM line profile across the terrace at the edge [Fig. 1(b)], which is about 10 nm, corresponding to ~7 monolayers of WTe_2. The $WTe_{1.5}$ and $WTe_{1.8}$ ultrathin films have the same thickness and similar roughness. The grain size of these ultrathin films is about 50 nm (see the supplementary material).

Figure 2(a) shows the XRD patterns of the WTe_2 ultrathin films, together with the standard diffraction patterns of the mica substrate for comparison. For the WTe_2 sample, in addition to the diffraction peaks coming from the mica substrate, other discernable peaks are all attributed to (00*l*) diffraction planes of WTe_2 single crystal, indicating that the film orientation is along the *c*-axis. The lattice constant deduced from (00*l*) peaks is $c = 1.403$ nm, consistent with the previous study.[20–22] $WTe_{1.5}$ and $WTe_{1.8}$ samples have the same patterns as those of WTe_2. The inset of Fig. 2(a) shows the digital photograph of the centimeter-scale WTe_2 ultrathin film.

Figure 2(b) shows the typical Raman spectra of ultrathin films with different annealing conditions, indicating the good crystalline ordering. To precisely determine the position of the peaks and the full width at half maximum (FWHM) value, each peak is fitted with a Lorentz curve. There are five dominant Raman-active peaks at around 109.6, 114.5, 132.2, 162.1, and 210.1 cm^{-1}, which are related to the A_2^4, A_1^9, A_1^8, A_1^5, and A_1^2 phonon modes, respectively.[23–29] As seen from Fig. 2(b), the Raman spectra of these samples show the apparent difference with different Te vapor pressures. As for $WTe_{1.8}$ and $WTe_{1.5}$ samples, with increasing Te vacancies, all the marked peaks show increased blueshift (~0.2–0.6 cm^{-1}) and broadening (FWHM: ~0.3–0.6 cm^{-1}). This is probably ascribed to the structural distortion due to the excessive Te vacancies in the film annealed in the lower Te vapor pressure. Te vacancies can be readily induced during the film growth where the vapor pressure of Te is much larger than that of W. Annealing in the appropriate Te vapor pressure can get rid of these structural defects and improve the crystal quality to some extent, yielding the five typical WTe_2 Raman vibrational peaks without any discernible peak shift.

We choose the WTe_2 and $WTe_{1.5}$ samples for the further transport study. Figure 3(a) shows the temperature-dependent resistance curves of $WTe_{1.5}$ and WTe_2 ultrathin films. It is well-known that the single-crystalline WTe_2 bulk sample should exhibit the well-defined metallic behavior and may turn to the insulating state below a certain thickness. Here,

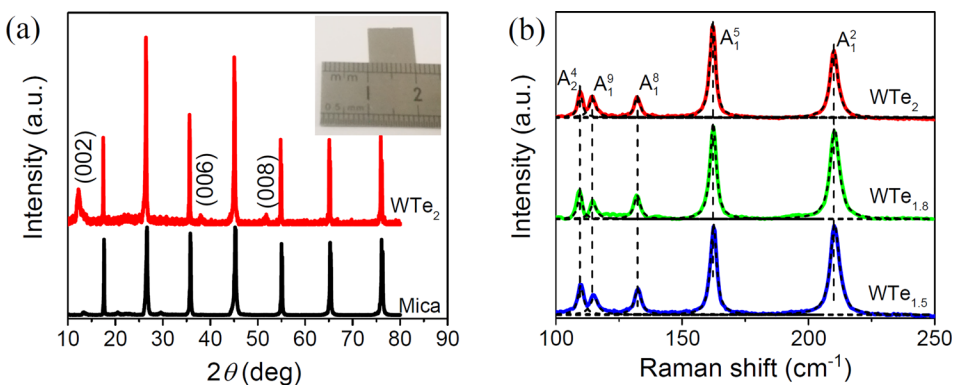

FIG. 2. Structural characterization of WTe_2 ultrathin films. (a) XRD patterns and (b) Raman spectra of $WTe_{1.5}$, $WTe_{1.8}$, and WTe_2 ultrathin films. Inset shows the digital photograph of the centimeter-scale WTe_2 sample.

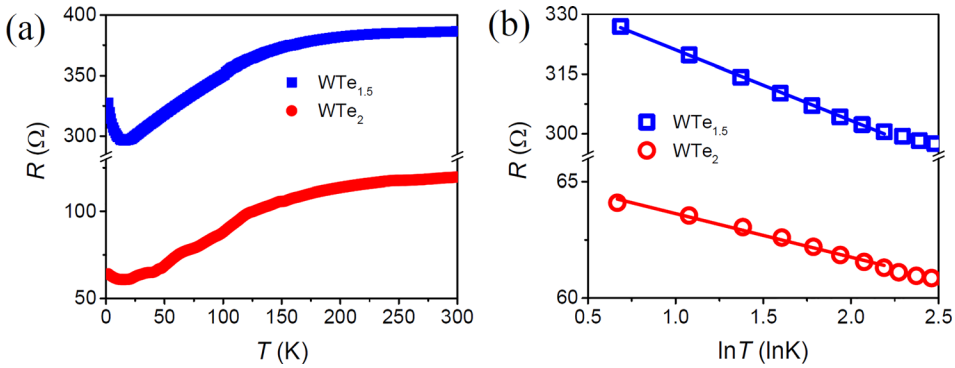

FIG. 3. (a) Temperature-dependent resistance of $WTe_{1.5}$ and WTe_2 ultrathin films. (b) The fitted low temperature *R-T* curves below the point of resistance minima in (a).

we find that both WTe_2 and $WTe_{1.5}$ show the metallic behavior, indicating their excellent crystal quality with thickness above the critical thickness. The $WTe_{1.5}$ sample has the lower residual resistivity ratio (RRR, which is defined as $RRR = \frac{\rho_{300K}}{\rho_{2K}}$) than the WTe_2 sample. This is probably due to the existence of the more content of Te vacancies,[14] consistent with the XPS and EDS composition measurements. The low-temperature resistivity minima are visible at around 10 K for the both ultrathin films, which is attributed to the weak localization in quantum interference effects as seen below. Figure 3(b) shows the linear fit for the $R \sim \ln T$ curve. The results show the resistance correction corresponding to a $\lambda \ln T$ relation, which is the typical signature of the weak localization effect.[30]

Figure 4(a) depicts the MR ($MR = \frac{R(B)-R_0}{R_0}$, R_0 is the resistance at zero field) curves measured at 2 K for both samples. The MR value of $WTe_{1.5}$ is much smaller than that of bulk WTe_2 crystals,[1] which is due to the lower mobility[31] and the imbalance of concentration between holes and electrons[14] in few layer samples. Meanwhile, the MR value is comparable to those of CVD-grown samples[14,32] and mechanical exfoliated samples with the similar thickness.[13] The MR value is comparable to another 100-nm-thick WTe_2 film, whose average mobility $\mu_{avg} = 730\,cm^2\,V^{-1}\,s^{-1}$ is obtained from the Lorentz law, $MR \approx (\mu_{avg} B)^2$ (see the supplementary material). The MR value becomes larger in the WTe_2 sample due to the suppression of Te vacancies. This agrees with the previous report that the MR value tends to dramatically decrease in the Te-deficient WTe_2 sample,[33] which also means that self-doping can be able to tune the MR ratio. Figure 4(c) shows the enlarged low-field curve of Fig. 4(a), in which both $WTe_{1.5}$ and WTe_2 samples have a positive MR cusp associated with weak antilocalization. The additional negative MR feature at the higher magnetic fields, associated with weak localization, denote the competition between weak antilocalization and weak localization. Compared with the $WTe_{1.5}$ sample, the weak localization of the WTe_2 sample becomes weaker. Also, it can be seen that the weak localization component fades quickly in the WTe_2 sample with the increasing measurement temperature [Fig. 4(b)], because the dephasing length decreases with an increase in temperature due to the increased inelastic-scattering, i.e., electron-phonon scattering and electron-electron scattering.

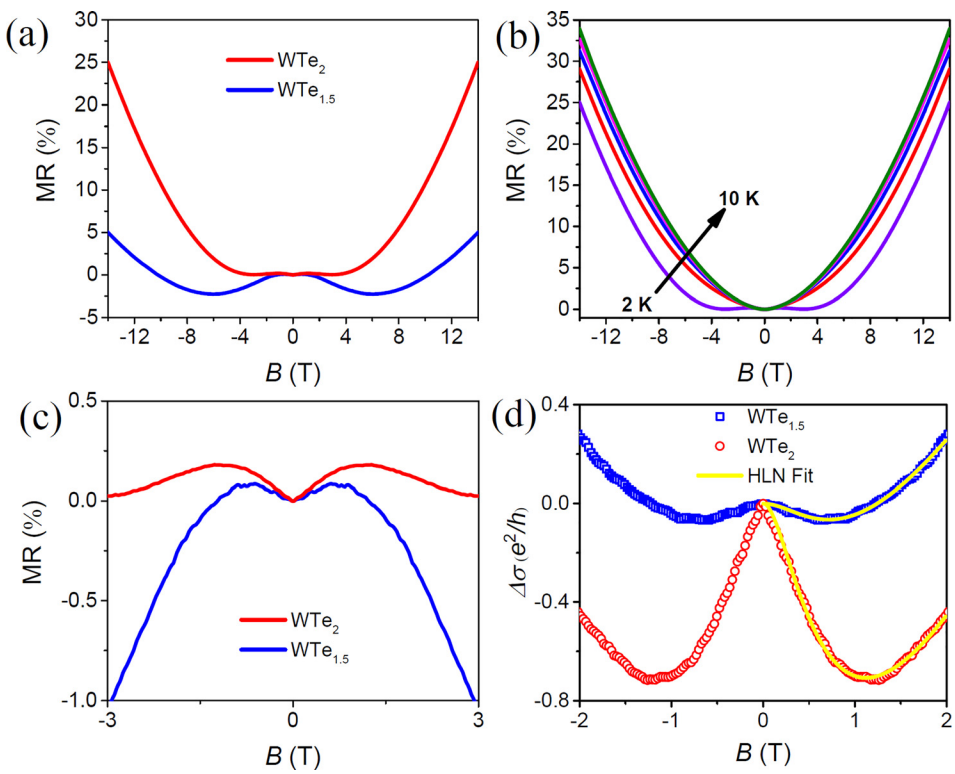

FIG. 4. (a) MR curves at 2 K of $WTe_{1.5}$ and WTe_2 ultrathin films. (b) Temperature-dependent MR curves of the WTe_2 sample. (c) The enlarged MR curves in the low-field region in (a). (d) The fitted magnetoconductance curves of $WTe_{1.5}$ and WTe_2 ultrathin films, as converted from their MR data.

To understand the difference of MR behavior between the $WTe_{1.5}$ and WTe_2 samples, we fit these MR curves by Hikami-Larkin-Nagaoka (HLN) equation,[34] which is written as,

$$\Delta\sigma(B) - \Delta\sigma(0) = \frac{e^2}{\pi h}\left\{\Psi\left(\frac{1}{2}+\frac{B_\varphi + B_{so}}{B}\right) + \frac{1}{2}\Psi\left(\frac{1}{2}+\frac{B_\varphi + 2B_{so}}{B}\right) - \frac{1}{2}\Psi\left(\frac{1}{2}+\frac{B_\varphi}{B}\right) - \ln\frac{B_\varphi + B_{so}}{B} - \frac{1}{2}\ln\frac{B_\varphi + 2B_{so}}{B} + \frac{1}{2}\ln\frac{B_\varphi}{B}\right\}. \quad (1)$$

where $\Psi(x)$ is digamma function. B_φ and B_{so} are the characteristic fields for dephasing and spin-orbit interaction, respectively. The characteristic fields are related to the characteristic lengths by $B_\varphi = \frac{\hbar}{4el_\varphi^2}$ and $B_{SO} = \frac{\hbar}{4el_{SO}^2}$, where the l_φ and l_{so} are the dephasing length and spin-orbit diffusion length, respectively, e is the electron charge, and $\hbar$ is the reduced Planck constant.

We fit the low-field MR curves of the $WTe_{1.5}$ and WTe_2 samples at 2 K in Eq. (1). The model fits the experimental results very well, as shown in Fig. 4(d). We extract two parameters B_φ and B_{so} of the $WTe_{1.5}$ sample, which are 0.32 and 0.30 T, respectively. While for the WTe_2 sample, the B_φ and B_{so} are 0.15 and 0.31 T, respectively. Interestingly, B_φ changed from 0.32 to 0.15 T, indicating the increase in the dephasing length from 22 to 33 nm. As the stoichiometry is changed from $WTe_{1.5}$ to WTe_2, the decrease in Te vacancies leads to the decrease in the inelastic scattering rate. Therefore, dephasing is suppressed with the decrease in Te vacancies, which is in correspondence with the increase in the dephasing length extracted from the above curve fitting. As a result, weak localization becomes weaker, and the competition of weak localization and weak antilocalization is modulated.

In summary, we have fabricated the centimeter-scale, uniform, and high-quality WTe_2 ultrathin films by combining PLD and the post-annealing technique. By annealing in the appropriate Te vapor pressure, we are able to improve the transport properties of WTe_2 by eliminating the Te vacancies. The MR value can reach the maximum of 25%, close to that of CVD-grown and mechanical foliated samples at the similar thickness. In addition, the WTe_2 ultrathin films undergo the competition between weak localization and weak antilocalization, which can be modulated by the amount of Te vacancies. Our work paves the way on the fabrication of high-quality, large-scale 2D materials for the practical device applications. WTe_2 fabrication on the mica substrate may help engineer the strain and shed light on testing whether the strained monolayer WTe_2 is a 2D topological insulator, as predicted.[35]

See supplementary material for stoichiometry of the $WTe_{2-\delta}$ ultrathin films, TEM characterization of a WTe_2 thin film, grains and grain boundaries of the WTe_2 ultrathin films, and mobilities and carrier densities of a 100-nm-thick WTe_2 film.

We gratefully acknowledge the financial support of the National Key Projects for Basic Research of China (Grant Nos. 2014CB921103, 2017YFA0206304 and 2017YFA0303200), the National Natural Science Foundation of China (Grant Nos. 91421109, 11274003, 11134005, 11522432, 61427812, and 11574288), the PAPD project, the Fundamental Research Funds for the Central Universities (Grant No. 021014380059), and Collaborative Innovation Center of Solid-State Lighting and Energy-Saving Electronics.

[1]M. N. Ali, J. Xiong, S. Flynn, J. Tao, Q. D. Gibson, L. M. Schoop, T. Liang, N. Haldolaarachchige, M. Hirschberger, N. P. Ong, and R. J. Cava, Nature **514**, 205 (2014).
[2]J. Jiang, F. Tang, X. C. Pan, H. M. Liu, X. H. Niu, Y. X. Wang, D. F. Xu, H. F. Yang, B. P. Xie, F. Q. Song, P. Dudin, T. K. Kim, M. Hoesch, P. K. Das, I. Vobornik, X. G. Wan, and D. L. Feng, Phys. Rev. Lett. **115**, 166601 (2015).
[3]F.-X. Xiang, M. Veldhorst, S.-X. Dou, and X.-L. Wang, Europhys. Lett. **112**, 37009 (2015).
[4]Z. Zhu, X. Lin, J. Liu, B. Fauque, Q. Tao, C. Yang, Y. Shi, and K. Behnia, Phys. Rev. Lett. **114**, 176601 (2015).
[5]X. C. Pan, X. Chen, H. Liu, Y. Feng, Z. Wei, Y. Zhou, Z. Chi, L. Pi, F. Yen, F. Song, X. Wan, Z. Yang, B. Wang, G. Wang, and Y. Zhang, Nat. Commun. **6**, 7805 (2015).
[6]D. Kang, Y. Zhou, W. Yi, C. Yang, J. Guo, Y. Shi, S. Zhang, Z. Wang, C. Zhang, S. Jiang, A. Li, K. Yang, Q. Wu, G. Zhang, L. Sun, and Z. Zhao, Nat. Commun. **6**, 7804 (2015).
[7]Y. Wu, D. Mou, N. H. Jo, K. Sun, L. Huang, S. L. Bud'ko, P. C. Canfield, and A. Kaminski, Phys. Rev. B **94**, 121113 (2016).
[8]K. F. Mak, C. Lee, J. Hone, J. Shan, and T. F. Heinz, Phys. Rev. Lett. **105**, 136805 (2010).
[9]S. Wang, H. Yu, H. Zhang, A. Wang, M. Zhao, Y. Chen, L. Mei, and J. Wang, Adv. Mater. **26**, 3538 (2014).
[10]J. Koo, Y. I. Jhon, J. Park, J. Lee, Y. M. Jhon, and J. H. Lee, Adv. Funct. Mater. **26**, 7454 (2016).
[11]D. MacNeill, G. M. Stiehl, M. H. D. Guimaraes, R. A. Buhrman, J. Park, and D. C. Ralph, Nat. Phys. **13**, 300 (2017).
[12]H. Ilatikhameneh, T. A. Ameen, G. Klimeck, J. Appenzeller, and R. Rahman, IEEE Electron Device Lett. **36**, 1097 (2015).
[13]L. Wang, I. Gutierrez-Lezama, C. Barreteau, N. Ubrig, E. Giannini, and A. F. Morpurgo, Nat. Commun. **6**, 8892 (2015).
[14]E. Zhang, R. Chen, C. Huang, J. Yu, K. Zhang, W. Wang, S. Liu, J. Ling, X. Wan, H. Z. Lu, and F. Xiu, Nano Lett. **17**, 878 (2017).
[15]Z. Yang and J. Hao, J. Mater. Chem. C **4**, 8859 (2016).
[16]C. R. Serrao, A. M. Diamond, S.-L. Hsu, L. You, S. Gadgil, J. Clarkson, C. Carraro, R. Maboudian, C. Hu, and S. Salahuddin, Appl. Phys. Lett. **106**, 052101 (2015).
[17]Y.-T. Ho, C.-H. Ma, T.-T. Luong, L.-L. Wei, T.-C. Yen, W.-T. Hsu, W.-H. Chang, Y.-C. Chu, Y.-Y. Tu, K. P. Pande, and E. Y. Chang, Phys. Stat. Sol. (RRL) **9**, 187 (2015).
[18]S. N. Grigoriev, V. Y. Fominski, R. I. Romanov, A. G. Gnedovets, and M. A. Volosova, Appl. Surf. Sci. **282**, 607 (2013).
[19]J. D. Yao, Z. Q. Zheng, J. M. Shao, and G. W. Yang, Nanoscale **7**, 14974 (2015).
[20]S. J. A. Mar and J. A. Ibers, J. Am. Chem. Soc. **114**, 8963 (1992).
[21]B. E. Brown, Acta Crystallogr. **20**, 268 (1966).
[22]P. L. Cai, J. Hu, L. P. He, J. Pan, X. C. Hong, Z. Zhang, J. Zhang, J. Wei, Z. Q. Mao, and S. Y. Li, Phys. Rev. Lett. **115**, 057202 (2015).
[23]Y. C. Jiang, J. Gao, and L. Wang, Sci. Rep. **6**, 19624 (2016).
[24]Y. Kim, Y. I. Jhon, J. Park, J. H. Kim, S. Lee, and Y. M. Jhon, Nanoscale **8**, 2309 (2016).
[25]W. D. Kong, S. F. Wu, P. Richard, C. S. Lian, J. T. Wang, C. L. Yang, Y. G. Shi, and H. Ding, Appl. Phys. Lett. **106**, 081906 (2015).
[26]C. H. Lee, E. C. Silva, L. Calderin, M. T. Nguyen, M. J. Hollander, B. Bersch, T. E. Mallouk, and J. A. Robinson, Sci. Rep. **5**, 10013 (2015).
[27]J. Lee, F. Ye, Z. Wang, R. Yang, J. Hu, Z. Mao, J. Wei, and P. X. Feng, Nanoscale **8**, 7854 (2016).
[28]Q. Song, X. Pan, H. Wang, K. Zhang, Q. Tan, P. Li, Y. Wan, Y. Wang, X. Xu, M. Lin, X. Wan, F. Song, and L. Dai, Sci. Rep. **6**, 29254 (2016).
[29]Q. Song, H. Wang, X. Xu, X. Pan, Y. Wang, F. Song, X. Wan, and L. Dai, RSC Adv. **6**, 103830 (2016).

[30]W. Niu, M. Gao, X. Wang, F. Song, J. Du, X. Wang, Y. Xu, and R. Zhang, Sci. Rep. **6**, 26081 (2016).
[31]X. Luo, C. Fang, C. Wan, J. Cai, Y. Liu, X. Han, Z. Lu, R. Xiong, and Z. Zeng, Nanotechnology **28**, 145704 (2017).
[32]J. Zhou, F. Liu, J. Lin, X. Huang, J. Xia, B. Zhang, Q. Zeng, H. Wang, C. Zhu, L. Niu, X. Wang, W. Fu, P. Yu, T. R. Chang, C. H. Hsu, D. Wu, H. T. Jeng, Y. Huang, H. Lin, Z. Shen, C. Yang, L. Lu, K. Suenaga, W. Zhou, S. T. Pantelides, G. Liu, and Z. Liu, Adv. Mater. **29**, 1603471 (2017).
[33]Y. Y. Lv, B. B. Zhang, X. Li, B. Pang, F. Zhang, D. J. Lin, J. Zhou, S. H. Yao, Y. B. Chen, S. T. Zhang, M. Lu, Z. Liu, Y. Chen, and Y. F. Chen, Sci. Rep. **6**, 26903 (2016).
[34]W. Knap, C. Skierbiszewski, A. Zduniak, E. Litwin-Staszewska, D. Bertho, F. Kobbi, J. L. Robert, G. E. Pikus, F. G. Pikus, S. V. Iordanskii, V. Mosser, K. Zekentes, and Yu. B. Lyanda-Geller, Phys. Rev. B **53**, 3912 (1996).
[35]X. Qian, J. Liu, L. Fu, and J. Li, Science **346**, 1344 (2014).